Data Repository for

Peneplain formation in southern Tibet predates India-Asia collision and plateau uplift

The material in this data repository includes information on the geomorphology of the investigated bedrock peneplain in the region of Bangoin (section 1) and the detailed analytical results of the geochronological investigations performed in this study (section 2).

1. Geomorphology of the bedrock peneplain

The bedrock peneplain in the northern Lhasa block is best preserved in the vicinity of the town Bangoin. To illustrate the morphology of the landscape in this region we present a digital elevation model (Fig. DR1A) and a figure that combines the spatial distribution of local slope angles with the local elevation (Fig. DR1B). In addition, we show three field photographs of the peneplain region (Fig. DR2A-C).

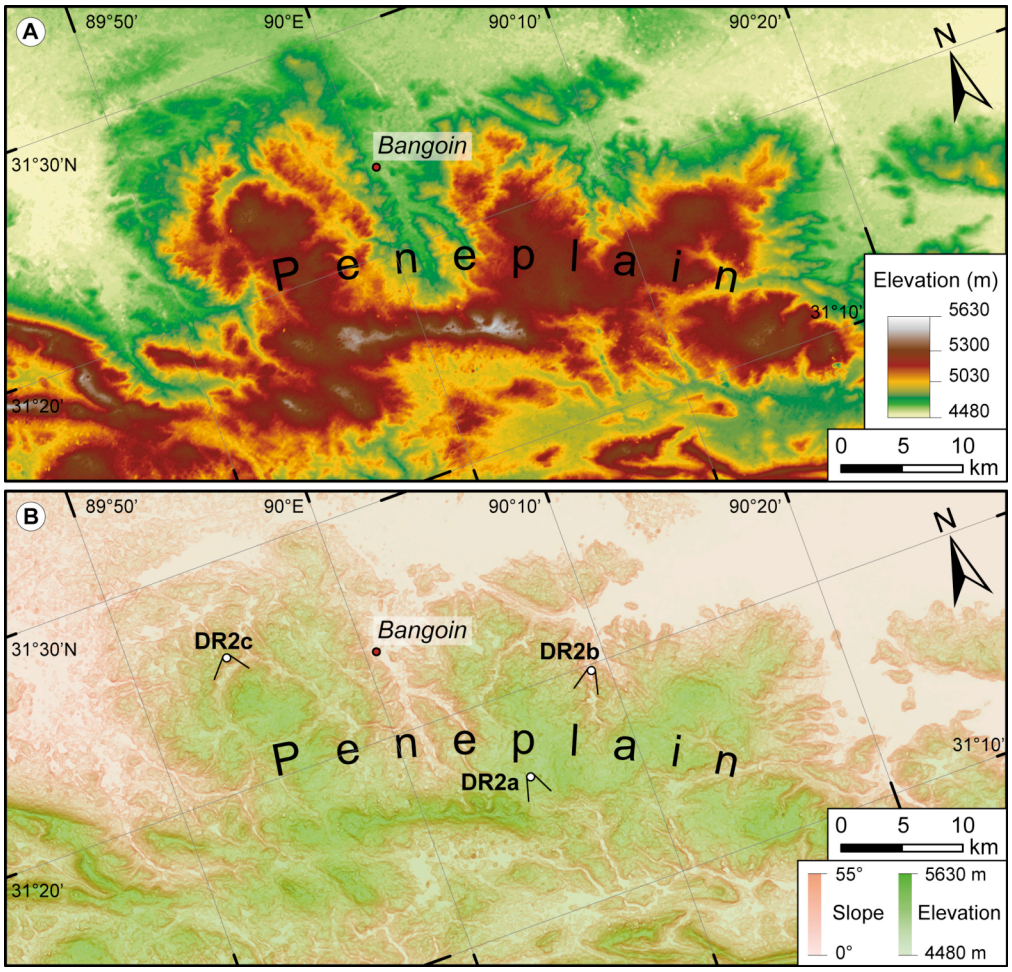

Figure DR1. A: Digital elevation model of the peneplain region near the town Bangoin. The peneplain surface, which is at an elevation of ~5300 m, appears in brownish colours. The digital elevation model is based on a Global Digital Elevation Model (GDEM) derived from ASTER GDEM data with a spatial resolution of ~30 m. **B:** Map of the region shown in (A) illustrating spatial variations in slope angle and elevation. Note that slope angles in the valleys dissecting the peneplain increase towards lower elevation. White circles mark the positions from which the photographs shown in Figure DR2 were taken (black lines mark the view direction).

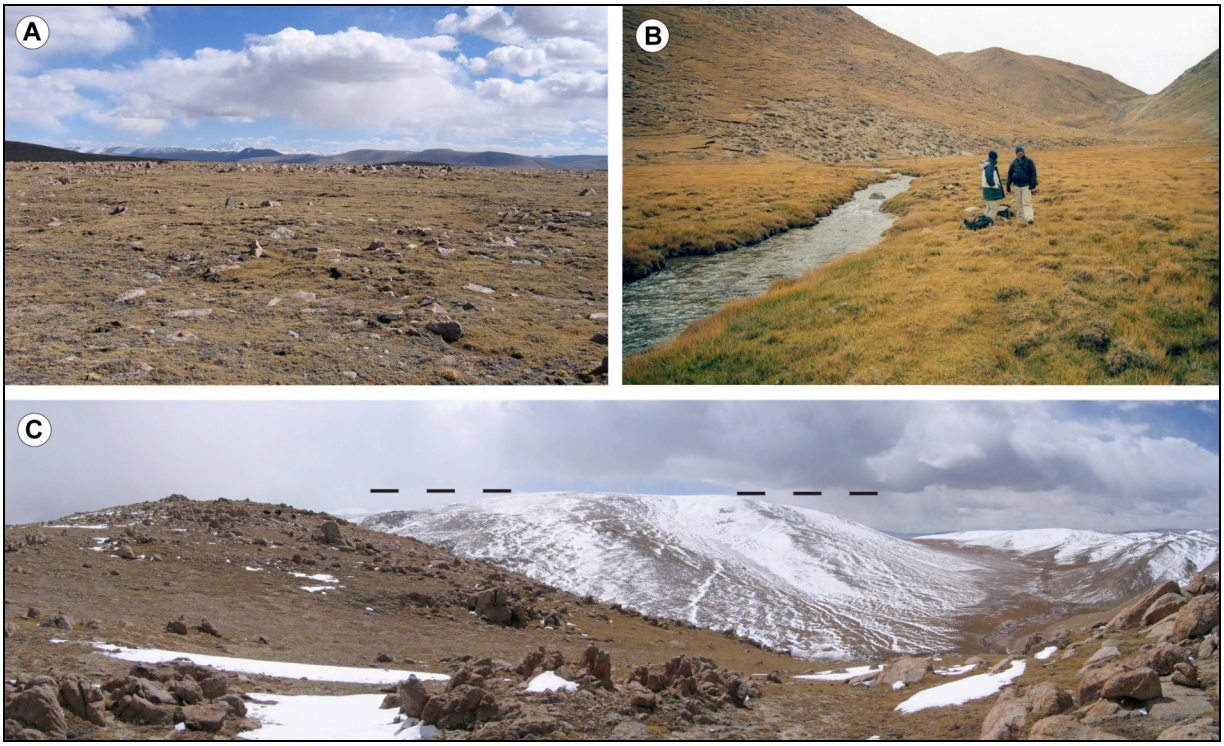

Figure DR2. Field photographs of the peneplain region (for location and view direction see Fig. DR1B). **A:** A well-preserved part of the flat peneplain southeast of Bangoin with granite blocks and a thin veneer of intervening soil. **B:** Small valley east of Bangoin that was incised into the peneplain by a stream flowing to the north. **C:** The peneplain – indicated by the dashed line – west of Bangoin where it has been incised by a river flowing to the northeast.

2. Description of the geochronological investigations

Below we outline the methods used to (1) date the intrusion of the granitoids with U/Pb zircon dating and (2) constrain their subsequent cooling history with (U-Th)/He dating of zircon and apatite, apatite fission track dating, and thermal modeling. In addition, we describe the derivation of local and catchment-wide erosion rates using *in situ*-produced cosmogenic ^{10}Be. The detailed analytical results are presented in six tables (Tables DR1–DR6).

2.1 U/Pb dating and low-temperature thermochronology

Zircon and apatite crystals were concentrated by standard mineral separation processes (crushing, sieving, gravity and magnetic separation). U/Pb age data were acquired by laser ablation—single collector—magnetic sectorfield— inductively coupled plasma—mass spectrometry (LA-SF-ICP-MS) at the Geological Survey of Denmark and Greenland in Copenhagen employing a ThermoFinnigan Element2 mass spectrometer coupled to a NewWave UP213 laser ablation system. All age data were obtained by single spot analyses with a spot diameter of 30 μm and a crater depth of approximately 15–20 μm. Cathodoluminescence imaging of each zircon was used to study internal structure and avoid ablation of heterogeneous zones. The methods employed for analysis and data processing are described in Frei and Gerdes (2009) and Gerdes and Zeh (2006). For quality control, the Plešovice (Sláma et al., 2008) and M127 (Nasdala et al., 2008) zircon standards were analyzed. The results were consistently within 1σ of the published ID-TIMS ages.

U/Pb ages were calculated with Isoplot/Ex 3.0 (Ludwig, 2003).

Apatite crystals for fission track analysis were irradiated at the research reactor of the Technical University of Munich (Garching). The external detector method (Gleadow, 1981) was used. After irradiation the induced fission tracks in the mica detectors were revealed by etching in 40% HF for 40 min at 21 °C. Tracks were counted with a Zeiss-Axioskop microscope – computer-controlled stage system (Dumitru 1993), with 1000x magnification. The fission track ages were determined by the zeta method (Hurford and Green, 1983) using age standards listed in Hurford (1998). Errors were calculated using double Poisson dispersion (Green, 1981). Calculations and plots were made with the program TRACKKEY (Dunkl, 2002).

For (U-Th)/He thermochronology only clear, intact, euhedral apatite and zircon single crystals were used. The shape parameters for the alpha ejection correction (Farley et al., 1996) were determined by multiple microphotographs. The crystals were wrapped in ca. 1x1 mm-sized platinum capsules and degassed in high vacuum by heating with an infrared laser in the Thermochronology Laboratory at Geoscience Center, University of Göttingen. The extracted gas was purified by a Ti-Zr getter and the He content was measured by a Hiden triple-filter quadrupol mass spectrometer. Following degassing, samples were retrieved from the gas extraction line and spiked with calibrated ^{230}Th and ^{233}U solutions. Zircons were dissolved in pressurized teflon bombs using distilled 48% HF + 65% HNO_3 in five days at 220 °C, while apatites were dissolved in 2% HNO_3 at room temperature in an ultrasonic bath. The concentrations of alpha-emitting elements (actinides and Sm) were determined by ICP-MS using isotope dilution.

The thermal histories of the samples were modelled with the HeFTy program (Ketcham, 2005). The modelling is based on AFT, AHe and ZHe apparent ages, track length distributions, Dpar values, apatite and zircon crystal dimensions, and U content. We have tested both multiple and averaged AHe grain data for the thermal modelling. As the average grain parameters gave more consistent results, we used the unweighted arithmetic mean of the ages, grain radii, and U and Th concentrations for thermal modeling. The annealing models used for AFT, AHe, and ZHe are described in Ketcham et al. (2007), Farley (2000), and Reiners et al. (2004), respectively. The thermal modelling was performed basically in 'unsupervised mode'. As fixed constraints we only used (i) the emplacement age the Bangoin intrusives (120 ± 10 Ma), (ii) a mean surface temperature of 5 °C, and (iii) a time interval for the deposition of the Eocene red beds of 50 to 40 Ma with a near-surface temperature of 15-20 °C for this time, because the red beds were deposited at tropical latitude. Note that the 50-40 Ma time constraint used for sediment deposition is a conservative approach because the red beds contain intercalated fine-grained tuffs, which are presumably related to the main phase of Linzizong volcanism around 50 Ma. Assuming a shorter age range near ~50 Ma would lead to an even higher rate of cooling and exhumation.

2.2 Determination of erosion rates from cosmogenic ^{10}Be

Before we describe the determination of the erosion rates from concentrations of cosmogenic ^{10}Be in quartz (Lal, 1991), we note that we use the term *erosion* to describe the surface lowering of a landscape. Strictly speaking, ^{10}Be concentrations record the rate of *denudation*, i.e. the sum of physical erosion and chemical weathering (Riebe et al., 2003). To quantify local erosion rates on the peneplain we used granitic bedrock samples and samples consisting of granite grus. The latter were taken over areas of 10–50 m^2 and amalgamate thousands of grains that record individual rock erosion histories, thus providing representative average erosion rates (Hancock and Kirwan, 2007; Meyer et al., 2010). To quantify catchment-wide erosion rates (Granger et al., 1996) we took sediment samples from small streams.

After crushing of the grus and bedrock specimens, all samples were washed, sieved, and the non-magnetic part of the 250–500 µm grain size fraction was used for further purification. Samples were leached once in 6M HCl and three to four times in a mixture of 1% HF and 1% HNO_3 at 80 °C in an ultrasonic bath. After addition of ~0.3 mg of Be carrier, the pure quartz samples were dissolved and Be was separated by successive anion and cation exchange columns. The Be in the eluate was precipitated as $Be(OH)_2$ at a pH of 8-9, rinsed, dried, and transformed to BeO at ~1000 °C. Finally, the BeO was mixed with copper powder and analysed by accelerator mass spectrometry at ETH Zurich. The accelerator mass spectrometry measurements at ETH Zurich were normalized to the standards S555 and S2007, which have $^{10}Be/^{9}Be$ ratios of 95.5×10^{-12} and 30.8×10^{-12}, respectively (Kubik and Christl, 2010), and are calibrated against the primary BEST433 standard (Hofmann et al., 1987). The ^{10}Be erosion rates were calculated with the CRONUS-Earth $^{10}Be - ^{26}Al$ calculator (Balco et al., 2008), version 2.2.1 (http://hess.ess.washington.edu), using the constant production rate scaling model of Lal (1991) – Stone (2000). The calculator uses a ^{10}Be half-life of 1.387 Ma (Chmeleff et al., 2010; Korschinek et al., 2010) and corrects for the different standards and Be half-life used at ETH Zurich. The erosion rates – given with internal and external uncertainties – are *maximum* rates as no correction for snow shielding was made (Lal, 1991).

REFERENCES CITED

Balco, G., Stone, J.O., Lifton, N.A., and Dunai, T.J., 2008, A complete and easily accessible means of calculating surface exposure ages or erosion rates from ^{10}Be and ^{26}Al measurements: Quaternary Geochronology, v. 3, p. 174–195.

Chmeleff, J., von Blanckenburg, F., Kossert, K., and Jakob, D., 2010, Determination of the ^{10}Be half-life by multicollector ICP-MS and liquid scintillation counting: Nuclear Instruments and Methods in Physics Research B, v. 268, p. 192–199.

Dumitru, T., 1993, A new computer-automated microscope stage system for fission-track analysis: International Journal of Radiation Applications and Instrumentation. Part D. Nuclear Tracks and Radiation Measurements, v. 21, no. 4, p. 575–580.

Dunkl, I., 2002, TRACKKEY: a Windows program for calculation and graphical presentation of fission track data: Computers and Geosciences, v. 28, no. 1, p. 3–12.

Farley, K.A., 2000, Helium diffusion from apatite: General behavior as illustrated by Durango fluorapatite: Journal of Geophysical Research, v. 105, p. 2903–2914.

Farley, K.A., Wolf, R.A., and Silver, L.T., 1996, The effects of long alpha-stopping distance on (U-Th)/He ages: Geochimica Cosmochimica Acta, v. 60, p. 4223–4229.

Frei, D., and Gerdes, A., 2009, Precise and accurate in situ U-Pb dating of zircon with high sample throughput by automated LA-SF-ICP-MS: Chemical Geology, v. 261, p. 261–270.

Gerdes, A., and Zeh, A., 2006, Combined U–Pb and Hf isotope LA-(MC)-ICP-MS analyses of detrital zircons: comparison with SHRIMP and new constraints for the provenance and age of an Armorican metasediment in Central Germany: Earth and Planetary Science Letters, v. 249, p. 47–61.

Gleadow, A.J.W., 1981, Fission-track dating methods: what are the real alternatives?: Nuclear Tracks, v. 5, p. 3–14.

Granger, D.E., Kirchner, J.W., and Finkel, R., 1996, Spatially averaged long-term erosion rates measured from in situ-produced cosmogenic nuclides in alluvial sediment: The Journal of Geology, v. 104, p. 249–257.

Green, P.F., 1981, A new look at statistics in fission track dating: Nuclear Tracks, v. 5, p. 77–86.

Hancock, G., and Kirwan, M., 2007, Summit erosion rates deduced from ^{10}Be: Implications for relief production in the central Appalachians: Geology, v. 35, p. 89–92.

Hofmann, H., Beer, J., Bonani, G., Von Gunten, H., Raman, S., Suter, M., Walker, R., Wölfli, W., and Zimmermann, D., 1987, ^{10}Be: Half-life and AMS standards: Nuclear Instruments and Methods in Physics Research B, v. 29, p. 32–36.

Hurford, A.J., 1998, Zeta: the ultimate solution to fission-track analysis calibration or just an interim measure?, *in* Van den Haute, P. and De Corte, F., eds, Advances in fission-track geochronology, Kluwer Academic Publishers, p. 19–32.

Hurford, A.J., and Green, P.F., 1983, The zeta age calibration of fission-track dating: Chemical Geology Isotope Geoscience Section, v. 41, p. 285–312.

Ketcham, R.A., 2005, Forward and Inverse Modeling of Low-Temperature Thermochronometry Data: Reviews in Mineralogy and Geochemistry, v. 58, p. 275-314.

Ketcham, R.A., Carter, A., Donelick, R.A., Barbarand, J. & Hurford, A.J., 2007, Improved modeling of fission-track annealing in apatite: American Mineralogist, v. 92, p. 799-810.

Korschinek, G., Bergmaier, A., Faestermann, T., Gerstmann, U., Knie, K., Rugel, G., Wallner, A., Dillmann, I., Dollinger, G., and von Gostomski, C., 2010, A new value for the half-life of ^{10}Be by Heavy-Ion Elastic Recoil Detection and liquid scintillation counting: Nuclear Instruments and Methods in Physics Research B, v. 268, p. 187–191.

Kubik, P.W., and Christl, M., 2010, ^{10}Be and ^{26}Al measurements at the Zurich 6 MV Tandem AMS facility: Nuclear Instruments and Methods in Physics Research B, v. 268, p. 880–883.

Lal, D., 1991, Cosmic ray labeling of erosion surfaces: *in situ* nuclide production rates and erosion models: Earth and Planetary Science Letters, v. 104, p. 424–439.

Ludwig, K.R., 2003, User's manual for Isoplot 3.00: a geochronological toolkit for Microsoft Excel. Berkeley Geochronology Center Special Publication, v. 4, 70 p.

Meyer, H., Hetzel, R., Fügenschuh, B., and Strauss, H., 2010, Determining the growth rate of topographic relief using in situ-produced ^{10}Be: A case study in the Black Forest, Germany: Earth and Planetary Science Letters, v. 290, p. 391–402.

Nasdala, L., Hofmeister, W., Norberg, N., Martinson, J., Corfu, F., Dörr, W., Kamo, S., Kennedy, A., Kronz, A., and Reiners, P., 2008, Zircon M257 – a homogeneous natural reference material for the ion microprobe U-Pb analysis of zircon: Geostandards and Geoanalytical Research, v. 32, p. 247–265.

Reiners, P.W., Spell, T.L., Nicolescu, S., and Zanetti, K.A., 2004, Zircon (U-Th)/He thermochronometry: He diffusion and comparisons with ^{40}Ar/^{39}Ar dating: Geochimica Cosmochimica Acta, v. 68, p. 1857–1887.

Riebe, C.S., Kirchner, J.W., and Finkel, R.C., 2003, Long-term rates of chemical weathering and physical erosion from cosmogenic nuclides and geochemical mass balance: Geochimica Cosmochimica Acta, v. 67, p. 4411–4427.

Sláma, J., Košler, J., Condon, D.J., Crowley, J.L., Gerdes, A., Hanchar, J.M., Horstwood, M.S.A., Morris, G.A., Nasdala, L., Norberg, N., Schaltegger, U., Schoene, B., Tubrett, M.N., and Whitehouse, M.J., 2008, Plešovice zircon – A new natural reference material for U–Pb and Hf isotopic microanalysis: Chemical Geology, v. 249, p. 1–35.

Stone, J.O., 2000, Air pressure and cosmogenic isotope production: Journal of Geophysical Research, v. 105, p. 23,753–23,759.

Table DR1. Location and lithology of geochronological samples

sample number	latitude (°N)	longitude (°E)	lithology
H-23	31.4227	89.8048	Granodiorite
H-24	31.4434	89.8054	Granodiorite
H-29	31.4433	89.8982	Biotite granite
H-30	31.4685	89.8959	Leucogranite
H-31	31.4797	89.9194	Leucogranite
DC-31	31.4677	89.9208	Biotite granite
DC-33	31.3733	90.0143	Granodiorite

Table DR2. Results of zircon U/Pb geochronology

H-23	U	Pb		RATIOS							AGES (Ma)				Cc[g]
spot#	(ppm)[a]	(ppm)[a]	Th/U[a]	$^{207}Pb/^{235}U$[b]	2 σ[d]	$^{206}Pb/^{238}U$[b]	2 σ[d]	rho[c]	$^{207}Pb/^{206}Pb$[e]	2 σ[d]	$^{207}Pb/^{235}U$	2 σ	$^{206}Pb/^{238}U$	2 σ	%
1	166	3	0.69	0.132	0.010	0.01853	0.00047	0.35	0.0515	0.0035	126	9	118	3	94
2	88	2	0.66	0.138	0.014	0.01981	0.00046	0.22	0.0507	0.0052	132	13	126	3	96
3	352	6	0.22	0.121	0.007	0.01750	0.00023	0.22	0.0499	0.0029	116	6	112	1	97
4	134	2	0.58	0.133	0.008	0.01820	0.00027	0.24	0.0529	0.0031	126	7	116	2	92
5	114	2	0.61	0.135	0.013	0.01916	0.00037	0.19	0.0511	0.0050	128	12	122	2	95
6	92	2	0.50	0.137	0.013	0.01968	0.00052	0.28	0.0506	0.0046	131	12	126	3	96
7	1216	22	0.07	0.125	0.002	0.01808	0.00016	0.52	0.0501	0.0007	120	2	116	1	97
8	134	3	0.47	0.142	0.011	0.01994	0.00042	0.27	0.0516	0.0039	135	10	127	3	95
9	105	2	0.53	0.135	0.016	0.01889	0.00034	0.15	0.0519	0.0062	129	14	121	2	94
10	134	3	0.56	0.134	0.012	0.01957	0.00052	0.29	0.0496	0.0043	127	11	125	3	98
11	968	19	0.09	0.135	0.004	0.01976	0.00025	0.42	0.0496	0.0013	129	4	126	2	98
12	485	9	0.27	0.132	0.009	0.01800	0.00038	0.33	0.0533	0.0033	126	8	115	2	91
13	172	3	0.88	0.145	0.021	0.01995	0.00034	0.12	0.0526	0.0076	137	19	127	2	93
14	847	18	0.24	0.151	0.007	0.02180	0.00030	0.31	0.0503	0.0021	143	6	139	2	97
15	3010	52	0.06	0.115	0.002	0.01731	0.00011	0.35	0.0482	0.0008	111	2	111	1	100
16	493	9	0.39	0.121	0.004	0.01829	0.00040	0.66	0.0479	0.0012	116	4	117	3	101
17	396	8	0.22	0.137	0.006	0.01976	0.00034	0.36	0.0503	0.0022	130	6	126	2	97
18	1535	37	0.08	0.164	0.004	0.02413	0.00018	0.27	0.0494	0.0013	155	4	154	1	99
19	1020	21	0.08	0.142	0.006	0.02012	0.00025	0.29	0.0513	0.0021	135	5	128	2	95
20	630	10	0.38	0.116	0.006	0.01620	0.00017	0.21	0.0519	0.0026	111	5	104	1	93
21	1752	35	0.06	0.138	0.004	0.02017	0.00023	0.39	0.0498	0.0014	132	4	129	1	98
22	129	2	0.57	0.125	0.010	0.01746	0.00025	0.19	0.0521	0.0040	120	9	112	2	93
23	113	2	0.69	0.142	0.014	0.01862	0.00026	0.14	0.0554	0.0056	135	13	119	2	88
24	621	12	0.09	0.133	0.008	0.01890	0.00029	0.25	0.0512	0.0030	127	7	121	2	95
25	693	13	0.37	0.127	0.007	0.01824	0.00017	0.17	0.0506	0.0027	122	6	117	1	96
											$^{206}Pb/^{238}U$	2 σ	n[f]	rej.[h]	
								Weighted mean age (Ma)			**117.0**	**2.8**	**23**	**1**	

Table DR2 continued

H-29	U	Pb		RATIOS							AGES (Ma)				Cc[g]
spot#	(ppm)[a]	(ppm)[a]	Th/U[a]	$^{207}Pb/^{235}U$[b]	2 σ[d]	$^{206}Pb/^{238}U$[b]	2 σ[d]	rho[c]	$^{207}Pb/^{206}Pb$[e]	2 σ[d]	$^{207}Pb/^{235}U$	2 σ	$^{206}Pb/^{238}U$	2 σ	%
2	401	7	0.56	0.120	0.008	0.0179	0.0008	0.68	0.0486	0.0025	115	7	114	5	99
3	544	16	0.39	0.227	0.017	0.0289	0.0010	0.45	0.0569	0.0039	208	14	184	6	88
4	770	13	0.42	0.117	0.004	0.0171	0.0004	0.58	0.0496	0.0015	112	4	109	2	97
5	99	2	0.55	0.133	0.017	0.0185	0.0005	0.22	0.0521	0.0064	127	15	118	3	93
6	246	5	0.27	0.123	0.007	0.0183	0.0005	0.47	0.0488	0.0024	118	6	117	3	99
7	232	4	0.32	0.113	0.008	0.0176	0.0006	0.45	0.0466	0.0030	109	8	113	4	103
8	339	6	0.25	0.113	0.010	0.0169	0.0007	0.44	0.0485	0.0038	109	9	108	4	99
9	216	4	0.31	0.125	0.009	0.0183	0.0004	0.33	0.0495	0.0032	120	8	117	3	98
10	381	7	0.13	0.125	0.008	0.0179	0.0003	0.24	0.0506	0.0030	119	7	114	2	96
11	1123	43	0.11	0.270	0.010	0.0382	0.0008	0.57	0.0513	0.0016	243	8	242	5	99
12	394	7	0.18	0.131	0.008	0.0187	0.0006	0.46	0.0508	0.0029	125	8	119	3	96
13	432	7	0.12	0.117	0.007	0.0172	0.0002	0.16	0.0494	0.0029	112	6	110	1	98
14	313	6	0.32	0.121	0.007	0.0178	0.0004	0.37	0.0492	0.0026	116	6	114	2	98
15	547	9	0.17	0.114	0.004	0.0168	0.0002	0.31	0.0490	0.0017	109	4	108	1	98
16	741	14	0.14	0.132	0.009	0.0186	0.0003	0.24	0.0514	0.0034	126	8	119	2	95
17	238	4	0.39	0.121	0.007	0.0182	0.0004	0.35	0.0484	0.0027	116	6	116	2	100
18	153	3	0.28	0.118	0.007	0.0166	0.0002	0.24	0.0518	0.0030	114	6	106	2	93
20	397	7	0.18	0.120	0.007	0.0176	0.0006	0.52	0.0496	0.0026	115	7	112	4	98
21	191	3	0.32	0.122	0.010	0.0174	0.0003	0.23	0.0510	0.0041	117	9	111	2	95
22	131	2	0.34	0.122	0.012	0.0174	0.0003	0.19	0.0508	0.0048	117	11	111	2	95
23	486	9	0.22	0.124	0.007	0.0183	0.0003	0.35	0.0492	0.0024	119	6	117	2	98
24	305	6	0.35	0.135	0.013	0.0203	0.0007	0.35	0.0481	0.0043	128	12	130	4	101
25	1040	18	0.61	0.120	0.003	0.0175	0.0001	0.28	0.0495	0.0012	115	3	112	1	98
26	87	2	0.66	0.139	0.016	0.0199	0.0006	0.25	0.0509	0.0057	133	14	127	4	96
27	125	2	0.63	0.132	0.016	0.0181	0.0004	0.19	0.0528	0.0064	126	15	116	3	92
											$^{206}Pb/^{238}U$	2 σ	n[f]	rej.[h]	
								Weighted mean age (Ma)			**111.7**	**1.6**	**23**	**2**	

Table DR2 continued

H-30	U	Pb		RATIOS							AGES (Ma)				Cc[g]
spot#	(ppm)[a]	(ppm)[a]	Th/U[a]	$^{207}Pb/^{235}U$[b]	2 σ[d]	$^{206}Pb/^{238}U$[b]	2 σ[d]	rho[c]	$^{207}Pb/^{206}Pb$[e]	2 σ[d]	$^{207}Pb/^{235}U$	2 σ	$^{206}Pb/^{238}U$	2 σ	%
1	275	5	0.16	0.121	0.007	0.0175	0.0003	0.27	0.0501	0.0028	116	6	112	2	97
4	186	3	0.29	0.124	0.008	0.0178	0.0002	0.20	0.0508	0.0032	119	7	114	1	95
5	876	15	0.15	0.115	0.009	0.0171	0.0002	0.18	0.0490	0.0036	111	8	109	1	98
6	207	4	0.32	0.124	0.009	0.0177	0.0004	0.27	0.0508	0.0036	119	8	113	2	95
7	113	3	0.22	0.195	0.014	0.0261	0.0014	0.78	0.0543	0.0024	181	12	166	9	92
8	335	6	0.41	0.129	0.010	0.0185	0.0003	0.22	0.0507	0.0038	124	9	118	2	96
9	242	4	0.47	0.122	0.010	0.0175	0.0005	0.33	0.0505	0.0040	117	9	112	3	96
11	442	15	0.28	0.236	0.009	0.0334	0.0007	0.51	0.0512	0.0017	215	8	212	4	98
14	386	16	0.26	0.309	0.019	0.0417	0.0007	0.27	0.0538	0.0031	274	14	263	4	96
15	658	12	0.21	0.133	0.008	0.0188	0.0006	0.52	0.0512	0.0025	126	7	120	4	95
16	442	8	0.16	0.123	0.010	0.0175	0.0004	0.29	0.0509	0.0040	118	9	112	3	95
18	66	4	1.75	0.525	0.027	0.0659	0.0017	0.50	0.0578	0.0025	429	18	412	10	96
19	327	6	0.21	0.126	0.009	0.0179	0.0005	0.36	0.0509	0.0035	120	8	114	3	95
21	648	44	0.40	0.523	0.020	0.0676	0.0014	0.54	0.0561	0.0018	427	13	422	8	99
23	344	14	0.55	0.288	0.014	0.0400	0.0007	0.38	0.0522	0.0023	257	11	253	5	98
24	432	9	0.40	0.152	0.008	0.0216	0.0005	0.45	0.0510	0.0025	144	7	138	3	96

	$^{206}Pb/^{238}U$	2 σ	n[f]	rej.[h]
Weighted mean age (Ma)	**112.8**	**2.3**	**11**	**2**

Table DR2 continued

DC-33	U	Pb		RATIOS							AGES (Ma)				Cc[g]
spot#	(ppm)[a]	(ppm)[a]	Th/U[a]	$^{207}Pb/^{235}U$[b]	2 σ[d]	$^{206}Pb/^{238}U$[b]	2 σ[d]	rho[c]	$^{207}Pb/^{206}Pb$[e]	2 σ[d]	$^{207}Pb/^{235}U$	2 σ	$^{206}Pb/^{238}U$	2 σ	%
1	76	1	0.67	0.117	0.012	0.0169	0.0005	0.28	0.0501	0.0048	112	11	108	3	96
2	50	1	0.56	0.127	0.015	0.0175	0.0005	0.25	0.0526	0.0060	121	14	112	3	92
3	95	2	0.82	0.122	0.007	0.0174	0.0003	0.31	0.0512	0.0028	117	6	111	2	95
4	64	1	0.65	0.118	0.014	0.0170	0.0003	0.13	0.0505	0.0061	114	13	109	2	96
5	108	2	0.63	0.118	0.011	0.0176	0.0003	0.17	0.0486	0.0045	113	10	113	2	99
6	48	1	0.68	0.127	0.016	0.0176	0.0005	0.22	0.0526	0.0065	122	14	112	3	92
7	75	1	0.67	0.121	0.014	0.0170	0.0005	0.23	0.0518	0.0058	116	13	109	3	93
8	55	1	0.59	0.124	0.020	0.0171	0.0005	0.17	0.0523	0.0083	118	18	110	3	93
9	128	2	0.65	0.122	0.008	0.0175	0.0003	0.27	0.0506	0.0033	117	7	112	2	96
10	111	2	0.68	0.124	0.010	0.0175	0.0006	0.39	0.0514	0.0040	119	9	112	4	94
11	73	1	0.80	0.129	0.014	0.0177	0.0005	0.27	0.0529	0.0055	123	13	113	3	92
12	90	2	0.69	0.123	0.009	0.0176	0.0004	0.30	0.0510	0.0037	118	8	112	3	95
13	93	2	0.45	0.125	0.016	0.0174	0.0003	0.14	0.0522	0.0065	120	14	111	2	93
14	81	1	0.43	0.112	0.014	0.0171	0.0006	0.30	0.0473	0.0057	108	13	110	4	102
15	43	1	0.66	0.118	0.016	0.0173	0.0005	0.20	0.0496	0.0066	113	15	110	3	97
16	100	2	0.74	0.118	0.011	0.0171	0.0004	0.28	0.0503	0.0045	114	10	109	3	96
17	48	1	0.49	0.131	0.023	0.0177	0.0006	0.18	0.0534	0.0092	125	21	113	4	91
18	144	3	0.52	0.121	0.008	0.0177	0.0003	0.27	0.0496	0.0033	116	8	113	2	98
19	135	2	0.44	0.119	0.008	0.0175	0.0004	0.32	0.0491	0.0032	114	7	112	2	98
20	91	2	0.83	0.118	0.014	0.0176	0.0004	0.19	0.0489	0.0059	114	13	112	3	99
21	133	2	0.97	0.123	0.008	0.0176	0.0003	0.27	0.0508	0.0034	118	8	112	2	95
22	115	2	0.59	0.135	0.023	0.0176	0.0003	0.11	0.0557	0.0094	129	21	112	2	87
23	64	1	0.42	0.120	0.014	0.0176	0.0004	0.21	0.0494	0.0056	115	12	112	3	98
24	123	2	0.51	0.120	0.008	0.0176	0.0005	0.43	0.0494	0.0029	115	7	112	3	98
25	236	4	0.33	0.117	0.007	0.0174	0.0005	0.44	0.0486	0.0027	112	6	111	3	99
26	321	6	0.28	0.151	0.073	0.0176	0.0004	0.05	0.0622	0.0299	143	64	112	3	79
27	190	3	0.33	0.124	0.006	0.0180	0.0002	0.23	0.0502	0.0023	119	5	115	1	96
28	138	2	0.47	0.117	0.014	0.0176	0.0005	0.25	0.0485	0.0055	113	13	112	3	100
29	136	2	0.91	0.120	0.010	0.0176	0.0005	0.35	0.0494	0.0037	115	9	112	3	98

	$^{206}Pb/^{238}U$	2 σ	n[f]	rej.[h]
Weighted mean age (Ma)	**111.6**	**0.5**	**29**	**2**

Table DR2 continued

DC-31	U	Pb		RATIOS							AGES (Ma)				Cc[g]
spot#	(ppm)[a]	(ppm)[a]	Th/U[a]	$^{207}Pb/^{235}U$[b]	2 σ[d]	$^{206}Pb/^{238}U$[b]	2 σ[d]	rho[c]	$^{207}Pb/^{206}Pb$[e]	2 σ[d]	$^{207}Pb/^{235}U$	2 σ	$^{206}Pb/^{238}U$	2 σ	%
1	521	10	0.15	0.129	0.006	0.0189	0.0004	0.42	0.0494	0.0020	123	5	121	2	98
2	235	4	0.36	0.125	0.004	0.0178	0.0002	0.30	0.0508	0.0017	119	4	114	1	95
4	497	10	0.11	0.136	0.006	0.0199	0.0004	0.45	0.0494	0.0020	129	6	127	3	98
7	674	49	0.54	0.564	0.015	0.0731	0.0008	0.39	0.0559	0.0014	454	10	455	5	100
9	553	10	0.18	0.120	0.008	0.0177	0.0006	0.51	0.0494	0.0029	115	7	113	4	98
10	227	13	0.35	0.511	0.016	0.0585	0.0009	0.52	0.0634	0.0017	419	11	366	6	87
11	482	27	0.46	0.443	0.020	0.0565	0.0013	0.48	0.0569	0.0023	373	14	354	8	95
12	131	13	0.82	0.856	0.037	0.0956	0.0018	0.44	0.0649	0.0025	628	20	589	11	94
14	357	23	0.40	0.505	0.021	0.0639	0.0016	0.61	0.0574	0.0019	415	14	399	10	96
16	867	16	0.07	0.122	0.011	0.0180	0.0003	0.20	0.0490	0.0044	117	10	115	2	99
19	343	7	0.49	0.154	0.009	0.0194	0.0005	0.44	0.0575	0.0029	145	8	124	3	85
20	449	12	0.47	0.186	0.010	0.0266	0.0003	0.24	0.0507	0.0026	173	8	169	2	98
21	298	18	0.68	0.483	0.026	0.0603	0.0015	0.46	0.0582	0.0028	400	18	377	9	94
23	359	7	0.40	0.135	0.008	0.0197	0.0005	0.40	0.0498	0.0026	129	7	126	3	98
24	404	8	0.32	0.138	0.008	0.0194	0.0005	0.47	0.0518	0.0025	132	7	124	3	94
25	332	6	0.32	0.125	0.005	0.0182	0.0004	0.50	0.0496	0.0018	119	5	116	2	98
											$^{206}Pb/^{238}U$	2 σ	n[f]	rej.[h]	
								Weighted mean age (Ma)			**117.5**	**3.9**	**10**	**1**	

[a] U and Pb concentrations and Th/U ratios are calculated relative to GJ-1 reference zircon.

[b] Corrected for background and within-run Pb/U fractionation and normalised to reference zircon GJ-1 (ID-TIMS values/measured value); $^{207}Pb/^{235}U$ calculated using ($^{207}Pb/^{206}Pb$)/($^{238}U/^{206}Pb$ * 1/137.88).

[c] Rho is the error correlation defined as the quotient of the propagated errors of the $^{206}Pb/^{238}U$ and the $^{207}/^{235}U$ ratio.

[d] Quadratic addition of within-run errors (2 SD) and daily reproducibility of GJ-1 (2 SD).

[e] Corrected for mass-bias by normalising to GJ-1 reference zircon (~0.6 per a.m.u.) and common Pb using the model of Stacey & Kramers (1975).

[f] Number of spots used for calculation.

[g] Concordance of $^{206}Pb/^{238}U$ and $^{207}Pb/^{235}U$.

[h] rej.: number of rejected acquisitions using isoplot (Ludwig, 2003).

Gray-dyed data were rejected, because the ages reflect an older zircon population or show inheritance.

Samples DC-31, H-29 and H-30 also yield a cluster of inherited zircons (>900 Ma) not listed in this table.

References

Ludwig, K.R., 2003, User's manual for Isoplot 3.00: a geochronological toolkit for Microsoft Excel. *Berkeley Geochronology Center Special Publication* 4, 70p.

Stacey, J.S., Kramers, J.D., 1975, Approximation of terrestrial lead isotope evolution by a two-stage model: *Earth and Planetary Science Letters,* 26, 207–221.

Table DR3. Results of zircon (U-Th)/He geochronology

		He		U-238			Th-232				Sm			Ejection	*Uncorr.*	**Ft-corr.**		**Sample**	
sample number	aliq.	vol. (ncc)	±1σ (ncc)	mass (ng)	±1σ (ng)	conc. (ppm)	mass (ng)	±1σ (ng)	conc. (ppm)	Th/U ratio	mass (ng)	±1σ (ng)	conc. (ppm)	correction (Ft)[a]	*He age (Ma)*	**age (Ma)**	**±1σ (Ma)**	**age[b] (Ma)**	**±1σ (Ma)**
H-23	#1	3.314	0.055	0.464	0.009	373	0.138	0.004	116	0.30	0.004	0.001	4	0.62	*55.0*	**89.2**	**±2.1**		
	#2	13.344	0.219	2.674	0.048	1576	0.130	0.003	80	0.05	0.005	0.001	4	0.66	*40.7*	**62.2**	**±1.5**		
	#3	11.802	0.194	1.740	0.031	878	0.231	0.006	117	0.13	0.006	0.001	3	0.68	*54.2*	**79.9**	**±1.9**	**77.1**	**±7.9**
H-24	#1	3.796	0.063	0.489	0.009	116	0.285	0.007	69	0.58	0.011	0.001	3	0.74	*56.3*	**76.5**	**±1.8**		
	#2	32.316	0.529	3.948	0.071	886	0.658	0.016	149	0.17	0.016	0.001	4	0.72	*64.9*	**90.2**	**±2.1**		
	#3	4.307	0.071	0.623	0.011	191	0.296	0.007	91	0.47	0.014	0.003	4	0.69	*51.3*	**74.0**	**±1.7**	**80.2**	**±5.0**
H-29	#1	9.584	0.158	1.690	0.031	1167	0.253	0.006	175	0.15	0.018	0.002	12	0.63	*45.2*	**71.3**	**±1.7**		
	#2	5.070	0.084	0.655	0.012	254	0.107	0.003	41	0.16	0.005	0.001	2	0.70	*61.5*	**88.0**	**±2.1**		
	#3	9.415	0.157	1.769	0.032	1140	0.163	0.004	105	0.09	0.012	0.002	8	0.65	*43.0*	**65.9**	**±1.6**	**75.1**	**±6.6**
H-30	#1	15.472	0.254	2.061	0.037	432	0.187	0.005	39	0.09	0.035	0.015	7	0.77	*60.6*	**78.9**	**±1.9**		
	#2	38.639	0.633	4.324	0.078	806	0.449	0.011	84	0.10	0.014	0.001	3	0.77	*71.8*	**93.0**	**±2.2**		
	#3	16.875	0.277	1.700	0.031	485	0.051	0.001	15	0.03	0.011	0.001	3	0.74	*81.1*	**110.3**	**±2.6**	**94.1**	**±9.1**
H-31	#1	15.807	0.260	2.921	0.053	1896	0.260	0.006	169	0.09	0.049	0.003	32	0.62	*43.8*	**71.0**	**±1.7**		
	#2	19.860	0.326	3.282	0.059	1107	0.234	0.006	79	0.07	0.057	0.003	19	0.72	*49.1*	**68.5**	**±1.6**		
	#3	23.931	0.392	4.613	0.083	2080	0.199	0.005	90	0.04	0.222	0.008	100	0.70	*42.4*	**60.5**	**±1.4**	**66.7**	**±3.2**
DC-31	#1	17.341	0.284	2.202	0.040	1064	0.495	0.012	239	0.22	0.059	0.011	29	0.68	*61.6*	**91.3**	**±2.1**		
	#2	8.313	0.137	1.303	0.024	836	0.126	0.003	81	0.10	0.007	0.001	4	0.64	*51.5*	**80.2**	**±1.9**		
	#3	6.803	0.112	1.043	0.019	810	0.233	0.006	181	0.22	0.030	0.003	23	0.51	*51.1*	**99.7**	**±2.3**		
	#4	26.202	0.429	3.873	0.070	1366	1.140	0.027	402	0.29	0.030	0.003	10	0.64	*52.2*	**81.8**	**±1.9**		
	#5	6.332	0.107	1.054	0.019	399	0.298	0.007	113	0.28	0.071	0.006	27	0.64	46.5	**72.4**	**±1.7**	**85.1**	**±4.7**
DC-33	#1	5.481	0.091	0.694	0.013	136	0.437	0.011	85	0.63	0.011	0.001	2	0.74	*56.7*	**76.5**	**±1.7**		
	#2	3.799	0.063	0.564	0.010	185	0.144	0.003	47	0.25	0.090	0.003	30	0.72	*52.3*	**73.1**	**±1.7**	**74.8**	**±1.7**

[a] alpha-ejection correction factor (Ft) after Farley et al. (1996).

[b] unweighted average age of each single Ft-corrected (U-Th)/He age.

Reference

Farley, K.A., Wolf, R.A., and Silver, L.T., 1996, The effects of long alpha-stopping distances on (U-Th)/He ages: Geochimica Cosmochimica Acta, v. 60, p. 4223–4229.

Table DR4. Results of apatite (U-Th)/He geochronology

		He		U-238			Th-232				Sm			Ejection	*Uncorr.*	**Ft-corr.**		**Sample**	
sample	aliq.	vol.	±1σ	mass	±1σ	conc.	mass	±1σ	conc.	Th/U	mass	±1σ	conc.	correction	*He age*	**He age**	**±1σ**	**age[b]**	**±1σ**
number		(ncc)	(ncc)	(ng)	(ng)	(ppm)	(ng)	(ng)	(ppm)	ratio	(ng)	(ng)	(ppm)	(Ft)[a]	*(Ma)*	**(Ma)**	**(Ma)**	**(Ma)**	**(Ma)**
H-23	#1	4.454	0.074	0.735	0.013	114	0.102	0.003	16	0.14	2.221	0.230	344	0.86	*47.3*	**55.1**	**±1.4**		
	#2	4.040	0.067	0.661	0.012	110	0.081	0.002	13	0.12	2.258	0.238	377	0.88	*47.7*	**54.4**	**±1.4**		
	#3	2.750	0.046	0.474	0.009	128	0.055	0.002	15	0.12	1.300	0.141	352	0.78	*45.6*	**58.6**	**±1.5**		
	#4	1.833	0.031	0.327	0.006	100	0.044	0.001	14	0.14	0.968	0.106	296	0.75	*43.8*	**58.1**	**±1.5**		
	#5	1.107	0.019	0.212	0.004	176	0.034	0.001	28	0.16	0.488	0.057	404	0.74	*40.7*	**54.9**	**±1.5**	**56.2**	**±0.9**
H-24	#1	0.622	0.011	0.092	0.002	20	0.045	0.001	10	0.49	1.553	0.150	343	0.81	*44.6*	**54.9**	**±1.6**		
	#2	0.454	0.009	0.066	0.001	23	0.034	0.001	12	0.51	1.074	0.105	376	0.79	*45.3*	**57.3**	**±1.7**		
	#3	0.230	0.005	0.042	0.001	16	0.021	0.001	8	0.50	0.510	0.052	195	0.65	*36.8*	**56.6**	**±1.9**	**56.3**	**±0.7**
H-29	#1	0.471	0.009	0.097	0.002	31	0.033	0.001	11	0.34	0.946	0.088	302	0.65	*34.4*	**52.7**	**±1.4**		
	#2	0.580	0.010	0.114	0.002	27	0.014	0.001	3	0.12	0.650	0.058	154	0.72	*39.2*	**55.9**	**±1.6**		
	#3	0.952	0.017	0.182	0.003	29	0.011	0.001	2	0.06	0.962	0.085	153	0.78	*40.7*	**52.2**	**±1.5**	**53.6**	**±1.2**
H-30	#1	0.260	0.005	0.054	0.001	45	0.005	0.001	4	0.09	0.344	0.017	280	0.62	*37.0*	**59.7**	**±1.8**		
	#2	0.095	0.003	0.011	0.001	4	0.005	0.001	2	0.47	0.457	0.023	188	0.78	*50.3*	**64.9**	**±3.8**		
	#3	0.715	0.013	0.126	0.002	5	0.010	0.001	1	0.08	1.087	0.054	43	0.82	*43.1*	**52.5**	**±1.4**	**59.0**	**±3.6**
H-31	#1	0.141	0.003	0.031	0.001	41	0.004	0.001	5	0.13	0.258	0.013	345	0.56	*34.3*	**61.0**	**±2.3**		
	#2	0.268	0.005	0.058	0.001	36	0.011	0.001	7	0.19	0.594	0.029	373	0.68	*33.8*	**49.7**	**±1.5**	**55.4**	**±5.7**
DC-31	#1	0.797	0.006	0.145	0.003	114	0.025	0.001	19	0.17	0.632	0.065	499	0.76	*42.2*	**55.7**	**±1.2**		
	#2	0.425	0.005	0.093	0.002	79	0.028	0.001	23	0.30	0.511	0.056	431	0.79	*33.8*	**42.6**	**±1.0**		
	#3	0.690	0.012	0.152	0.003	118	0.013	0.001	10	0.08	0.435	0.035	337	0.58	*35.9*	**61.4**	**±1.9**		
	#4	2.975	0.050	0.487	0.009	95	0.036	0.001	7	0.07	1.661	0.135	325	0.81	*48.2*	**59.3**	**±1.6**		
	#5	1.223	0.021	0.229	0.004	84	0.025	0.001	9	0.11	0.941	0.077	344	0.74	*41.7*	**56.3**	**±1.4**	**55.1**	**±3.3**
DC-33	#1	2.834	0.013	0.551	0.010	93	0.119	0.003	20	0.22	2.228	0.102	377	0.76	*39.2*	**51.8**	**±0.9**		
	#2	2.669	0.012	0.518	0.009	129	0.090	0.002	22	0.17	1.546	0.069	385	0.77	*39.9*	**51.6**	**±0.9**		
	#3	2.192	0.011	0.422	0.008	87	0.132	0.003	27	0.31	2.293	0.106	470	0.74	*38.4*	**51.9**	**±0.9**		
	#4	1.265	0.008	0.257	0.005	77	0.030	0.001	9	0.12	1.133	0.056	339	0.73	*38.3*	**52.7**	**±0.9**	**52.0**	**±0.2**

[a] alpha-ejection correction factor (Ft) after Farley et al. (1996).

[b] unweighted average age of each single Ft-corrected (U-Th)/He age.

Reference

Farley, K.A., Wolf, R.A., and Silver, L.T., 1996, The effects of long alpha-stopping distances on (U-Th)/He ages: Geochimica Cosmochimica Acta, v. 60, p. 4223–4229.

Table DR5. Results of apatite fission track geochronology and goodness of fit values from thermal modeling

sample	number of	spontaneous		induced		dosimeter		chi-square[d]	dispersion[e]	**central age[f]**	**±1σ**	U	Dpar	±1σ	GOF[g]	GOF[g]	GOF[g]
number	crystals	Rho[a]	(N)[b]	Rho[a]	(N)[b]	Rho[c]	(N)[c]	P (%)		**(Ma)**	**(Ma)**	(ppm)	(μm)	(μm)	(age)	(length)	(AHe)
H-23	24	40.0	(1918)	77.7	(3726)	7.13	(6715)	79	0.00	**59.4**	**±2.3**	129	2.90	±0.15	0.75	0.33	0.25
H-24	23	11.0	(648)	21.7	(1279)	7.14	(6715)	99	0.00	**58.5**	**±3.3**	35	2.49	±0.16	0.18	0.17	0.19
H-29	26	15.3	(943)	31.1	(1921)	7.15	(6715)	100	0.00	**56.8**	**±2.8**	51	2.59	±0.18	0.97	0.37	0.44
H-31	23	12.7	(632)	21.5	(1073)	7.18	(6715)	95	0.00	**68.4**	**±3.9**	35	2.47	±0.18	–	–	–
DC-31	24	14.1	(802)	28.5	(1621)	7.35	(6680)	96	0.00	**58.8**	**±3.0**	48	2.09	±0.20	0.27	0.28	0.26
DC-33	28	21.2	(1694)	45.0	(3589)	7.80	(7096)	92	0.00	**59.6**	**±2.4**	70	2.37	±0.18	–	–	–

[a] Track densities (Rho) are as measured ($x10^5$ tr/cm^2).

[b] Number of tracks counted is shown in brackets.

[c] Rho and N are track densities of the CN5 detector.

[d] Chi-square P(%): probability obtaining Chi-square value for n degree of freedom (where n = no. crystals – 1).

[e] Dispersion was determined according to Galbraith and Laslett (1993).

[f] Central ages were calculated using dosimeter glass CN5.

[g] Goodness of fit (GOF) values obtained from the thermal modeling with the HeFTy software (see Data Repository for details)

Reference

Galbraith, R.F., and Laslett, G.M., 1993, Statistical models for mixed fission track ages: International Journal of Radiation Applications and Instrumentation, Part D, Nuclear Tracks and Radiation Measurements, v. 21(4), p. 459–470.

Table DR6. Sample locations, ^{10}Be concentrations, and erosion rates

sample number	latitude (°N)	longitude (°E)	elevation (m)	mean elevation (m)	sample thickness (cm)	^{10}Be concentration[a] (10^4 at g^{-1})	production rate (muons) (at g^{-1} a^{-1})	production rate (spallation) (at g^{-1} a^{-1})	**Erosion rate[b] (m Ma^{-1})**	internal 1σ error (m Ma^{-1})	external 1σ error (m Ma^{-1})	time scale[c] (ka)
Grus samples[d]												
08T10	31.2690	90.0759	5306	-	-	912 ± 27	0.829	93.14	**6.58**	±0.21	±0.62	91
08T12	31.2741	90.0842	5351	-	-	906 ± 27	0.838	94.99	**6.76**	±0.21	±0.63	89
08T13	31.2703	90.0852	5358	-	-	951 ± 29	0.840	95.26	**6.44**	±0.20	±0.60	93
08T20	31.2747	89.8416	5109	-	-	534 ± 16	0.792	85.42	**10.54**	±0.33	±0.96	57
08T24	31.4293	89.9033	5203	-	-	838 ± 25	0.810	89.55	**6.91**	±0.22	±0.64	87
Bedrock samples												
08T16	31.4548	89.9809	4916	-	3.5	714 ± 21	0.738	78.85	**6.97**	±0.22	±0.65	86
08T25	31.4293	89.9033	5203	-	5.0	709 ± 21	0.783	89.55	**7.90**	±0.25	±0.73	76
Stream sediment samples[d]												
08T21	31.4854	89.9299	4688	5070	-	346 ± 10	0.785	84.30	**16.29**	±0.50	±1.5	37
08T23	31.4009	90.0009	4734	4921	-	487 ± 15	0.758	78.52	**10.66**	±0.33	±0.97	56
08T26	31.4475	89.8987	4893	5054	-	441 ± 13	0.782	83.66	**12.61**	±0.39	±1.1	48
09T21	31.3534	89.8542	4783	5193	-	408 ± 12	0.808	88.74	**14.47**	±0.45	±1.3	41
09T26	31.3224	90.0513	4804	5202	-	479 ± 14	0.810	88.96	**12.30**	±0.38	±1.1	49
09T27	31.3450	90.0392	4776	5169	-	522 ± 16	0.804	87.70	**11.09**	±0.34	±1.0	54

[a] Blank-corrected ^{10}Be concentrations. Propagated analytical errors (1σ) include the error based on counting statistics and the error of the blank correction.

[b] Erosion rates were calculated with the CRONUS-Earth ^{10}Be - ^{26}Al calculator, version 2.2.1 (Balco et al., 2008; http://hess.ess.washington.edu) assuming a rock density of 2.7 g cm^{-3} and using the constant production rate scaling model of Lal (1991) - Stone (2000). Internal uncertainties include errors from the counting statistics and the blank correction, whereas external uncertainties also include the error of the production rate introduced by the scaling model. For calculating catchment-wide denudation rates we used the mean elevation of the respective catchments, which is reported in column 5. Topographic shielding of all samples was negligible.

[c] The time over which the erosion rate integrates is calculated by dividing the absorption depth scale of 60 cm with the erosion rate.

[d] For determining local and catchment-wide erosion rates from grus and stream sediment samples we used the 0.5–2 mm and 0.25–0.5 mm grain size fractions, respectively. To correct for the topographic shielding of the catchments we calculated a shielding factor for each catchment from a 30 m digital elevation model with the Matlab script of Greg Balco (http://depts.washington.edu/cosmolab/P_by_GIS.html).